Analysis of Steady-State Reaction Fronts in a Porous Medium

F. Escobedo and H. J. Viljoen
Dept. of Chemical Engineering, University of Nebraska, Lincoln, NE 68588

A pseudohomogeneous model is used to analyze the steady state of a sharp reaction front in a porous medium. The reaction rate is described by the flame sheet approximation, and an asymptotic matching analysis is used to determine the temperature, conversion and position of the reaction front. Both adiabatic and nonadiabatic operations are considered, and the effect of radiation is included in the adiabatic case. The results show that there exists a maximum molar flux before blowout occurs. The critical molar flux is decreased by higher activation energies, but it is increased by higher rate constants and flame temperatures. Radiation further stabilizes the flame against blowout. Expressions are provided for the flame temperature, reactant conversion and the conditions when blowout occur. It is also shown that under certain conditions the front has two steady-state positions.

Introduction

Reactions in porous media form an important part of several technologies. Examples of reactions in porous media are found in catalytic reactors, gas-solid combustion synthesis (SHS), coal gasification, combustion in oil shale, catalyst regeneration, and porous radiant burners (PRB). Interactions among flow, reactant, and heat transfer in the presence of a highly exothermic reaction can lead to complex behavior. Once ignited, the reaction front can move upstream or downstream or stabilizes itself at some position. Wave propagation in combustion systems is a phenomenon that is well studied, and the theoretical basis of these waves was described by Marquardt (1989). A numerical approach was followed by Gatica et al. (1987) who solved the problem of traveling waves in nonadiabatic packed-bed reactors. They also provided *a-priori* expressions for the velocity of upstream or downstream traveling waves. An analytical approach to analyze this problem usually follows the method of matched asymptotics. The high activation energy of the combustion reaction limits the reaction to a thin zone, and matching the asymptotics of the solution inside the flame sheet with the solution outside the flame sheet leads to expressions for the flame temperature and position as a function of the other parameters of the system. This method was successfully applied to other combustion problems (cf. Matkowsky and Sivashinsky, 1979), and it is also the method that will be followed in this work. Norbury and Stuart (1989) also made use of matched asymptotics to analyze combustion in a porous medium.

Normally catalytic reactors are operated in the kinetic regime (Hlavacek, 1970), but there are exceptions where the reactions are carried out in the ignited state. Examples of these operations are the catalytic oxidation of carbon monoxide, methane and the synthesis of HCN. The bed is shallow, because the front is thin and the conversion is high. Apart from problems with blowout (that is, the front is not stabilized within the bed), continuous changes in the position of the front can lead to mechanical failure of the support materials (Thiart et al., 1991, 1993). Another technology that is closely related to this is porous radiant burners (PRB). Porous radiant burners made from ceramic materials or wire mesh are used to support a flame and convert a high fraction of the chemical energy into radiant energy which can be used to heat the load. The results of this work have only a limited application to a PRB, since the heat transfer to the load is not considered here.

A generic configuration for these systems consists of a porous medium of total length L_{tot}. Only the axial dimension x is considered. A premixed gas stream is fed into the system at $x=-L_1$ and flows toward the reaction front that is located at the position $x=0$ inside the porous medium. In this article, the model is discussed, as well as the matched asymptotic analysis for two cases. The adiabatic case with radiation is considered, and then the nonadiabatic case is analyzed and the condition for flame position is derived. Numerical results for

Correspondence concerning this article should be addressed to H. J. Viljoen.

a catalytic and a noncatalytic reaction are compared with the analytical results.

The Model

The model used in this analysis is based on a pseudohomogeneous description. Whereas packed bed reactors have typical porosity factors of 0.4, porous radiant burners operate on the far end of the scale for porosity, $\epsilon \approx 0.8-0.9$ using reticulated alumina or wire mesh. Golombok et al. (1990) proposed a correlation for the heat-transfer coefficient between the solid phase and the gas phase in a packed bed. When the heat-transfer coefficient and transfer area between the two phases are large, the use of a pseudohomogeneous model is justified. In this work, we assume that thermal equilibrium exists between the two phases. The steady-state temperature profile is described by:

$$\frac{d}{dx}\left(k_e\frac{dT}{dx}+4\phi\sigma_B d_p T^3\frac{dT}{dx}\right)-\rho_g C_p U\epsilon\frac{dT}{dx} -\frac{4h}{d}[T-T_{in}]+(-\Delta H)C\epsilon k_0 e^{-E/RT}=0 \quad (1)$$

Correlations can be used to evaluate the effective conductivity k_e (Hlavacek, 1970). Radiation is described by the diffusion model (cf. Norbury and Stuart, 1989; Vortmeyer, 1980). The use of the diffusion model to describe radiation is acceptable as long as the medium can be considered as optically dense (Sparrow and Cess, 1970). If the condition of optical density does not hold, alternative models should be used (Viskanta and Menguc, 1989).

The gas velocity U is calculated from the continuity equation:

$$\frac{d(\rho U)}{dx}=0. \quad (2)$$

Since ρU is constant ahead of the front and it is equal to the molar flux,

$$\rho U=\frac{G}{\epsilon}=\rho_{\text{in}}U_{\text{in}}. \quad (3)$$

The equation of state for the gas phase is taken as the ideal gas law:

$$\rho=\frac{\Pi}{RT} \quad (4)$$

Note that the gas phase is compressible. The length of the bed ranges from 0.04 m for porous burners to 0.30 m for packed-bed reactors (that is, for reactors operating in the ignited state), and the gas velocity is usually low. The pressure drop across the bed under such conditions will not be high and we will take Π as the average pressure across the bed (see also Gatica et al. 1987; Sathe et al., 1990). The reaction rate is assumed to be first-order with respect to the reactant concentration C, and the component balance is given by:

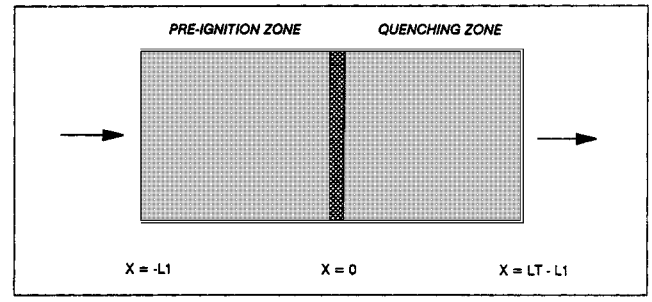

Figure 1. Reacting system.

$$-\frac{dUC}{dx}-k_0 Ce^{-E/RT}=0. \quad (5)$$

Reactant diffusion is omitted, because convection is the dominant mode of transfer.

The system in Figure 1 shows that the gas enters the reactor at $x=-L_1$ with a fixed inlet concentration, and for the energy balance the Danckwert's inlet boundary condition is used:

$$C=w_{\text{in}}\frac{\Pi}{RT} \quad (6)$$

$$k_e\frac{dT}{dx}=GC_p[T-T_{\text{in}}]. \quad (7)$$

Preheating occurs in the section $-L_1<x<0$. At the outlet we will use the Neumann condition:

$$\frac{dT}{dx}=0. \quad (8)$$

Since species diffusion is omitted, neither an outlet boundary condition nor an inlet condition of Danckwert's type can be used.

Analysis

When the activation energy of the reaction is large, the reaction zone will be thin, and on the scale of the bed length the zone can be approximated by a delta function. The role of the activation energy in switching the reaction on or off is well described by Norbury and Stuart (1989). This forms the basis for the analysis of most combustion and/or ignited reactions.

Adiabatic system

This approximation renders the equations exactly solvable outside the front for the adiabatic case. The solution of Eq. 1 ahead of the front is:

$$-cx=b\left[T_{\text{in}}^2(T_m-T)+\frac{T_{\text{in}}}{2}(T_m^2-T^2) +\frac{1}{3}(T_m^3-T^3)\right]+(k_e+bT_{\text{in}}^3)\ln\left(\frac{T_m-T_{\text{in}}}{T-T_{\text{in}}}\right) \quad (9)$$

where

$$b = 4\phi\sigma_B d_p \tag{10}$$

$$c = \rho C_p U \epsilon. \tag{11}$$

T_m denotes the temperature at the reaction front. Note that if $b = 0$ (neglecting the radiation contribution), then Eq. 9 can be solved explicitly for T to yield:

$$T = T_{\text{in}} + (T_m - T_{\text{in}}) e^{c/k_e x}. \tag{12}$$

The solution of Eq. 1 behind the front ($x > 0$) becomes:

$$T = T_m \tag{13}$$

$$C = w_{\text{out}} \frac{\Pi}{RT_m}. \tag{14}$$

Note that we do not assume complete conversion in the reaction zone. The question immediately arises why the reaction does not continue behind the front, and actually post-front combustion is observed in most SHS reactions. It, however, can be shown that in the case of an adiabatic reactor with an irreversible exothermic reaction, two solutions can exist. In the first one the reaction front is close to the inlet, and in the second one the reaction front is close to the outlet.

To extract more information from the system, it is necessary to analyze the flame zone. To do this, we will first define the parameter γ:

$$\gamma = \frac{E}{RT_m}. \tag{15}$$

This parameter will be large for high activation energy systems, and its inverse will subsequently be used as an expansion parameter to analyze the reaction zone. The temperature, velocity, and fuel concentration in the flame sheet are expanded in terms of $1/\gamma$, and the distance x is stretched as:

$$v = x\gamma \tag{16}$$

$$T_f = T_{f0} + \frac{1}{\gamma} T_{f1} + \ldots \tag{17}$$

$$C_f = C_{f0} + \frac{1}{\gamma} C_{f1} + \ldots \tag{18}$$

$$U_f = U_{f0} + \frac{1}{\gamma} U_{f1} + \ldots \tag{19}$$

These forms are substituted in Eqs. 1-5 and, considering only terms of the same order, will give an array of equations. Collecting terms of 0(1) gives:

$$\frac{d^2 T_{f0}}{dv^2} = 0. \tag{20}$$

The inner solutions must be matched with the outer solutions behind and ahead of the front. If the outer solutions are expressed in terms of the inner variable v, the solutions can be expanded in terms of $1/\gamma$. To illustrate this point, consider Eq. 9. Substituting v/γ for x, the solution is:

$$T = T_m + \frac{1}{\gamma} \frac{c(T_m - T_{\text{in}})}{k_e + bT_m^3} v + \ldots \tag{21}$$

The slope of the outer solution is:

$$\frac{dT}{dv} = 0 + \frac{1}{\gamma} \frac{c(T_m - T_{\text{in}})}{k_e + bT_m^3}. \tag{22}$$

When the solution of Eq. 20 is matched with the outer solutions, we get:

$$T_{f0} = T_m. \tag{23}$$

The next order of equations are:

$$k_e^* \frac{d^2 T_{f1}}{dv^2} + \epsilon(-\Delta H) C_{f0} k_0^* e^{-E/RT_{f0}} \cdot e^{T_{f1}/T_{f0}} = 0 \tag{24}$$

$$-\frac{GRT_{f0}}{\Pi} \frac{dC_{f0}}{dv} = \epsilon C_{f0} k_0^* e^{-E/RT_{f0}} \cdot e^{T_{f1}/T_{f0}} \tag{25}$$

where

$$k_e^* = k_e + bT_{f0}^3 \tag{26}$$

$$k_0^* = \frac{k_0}{\gamma}. \tag{27}$$

The boundary conditions for the inner temperature solution are determined by matching the inner and outer temperatures and first derivatives. When $v \to -\infty$:

$$T_{f1} \to -\infty, \quad \frac{dT_{f1}}{dv} = \beta \tag{28}$$

where

$$\beta = \frac{c(T_m - T_{\text{in}})}{k_e + bT_m^3}.$$

In the limit $v \to +\infty$ the boundary conditions are:

$$T_{f1} = 0, \quad \frac{dT_{f1}}{dv} = 0. \tag{29}$$

The values of C_{f0} when $v \to -\infty$ and $+\infty$, respectively, are given by:

$$C_{f0} = w_{\text{in}} \frac{\Pi}{RT_{f0}} \tag{30}$$

$$C_{f0} = w_{\text{out}} \frac{\Pi}{RT_{f0}}. \tag{31}$$

After substituting the reaction term from Eq. 25 into Eq. 24,

it can be integrated between v and $+\infty$ to give after rearranging terms:

$$C_{f0}=\frac{k_e^*\Pi}{(-\Delta H)GRT_{f0}}\left[\frac{dT_{f1}}{dv}+\frac{(-\Delta H)}{k_e^*}Gw_{\text{out}}\right]. \quad (32)$$

Taking the limit for $v\rightarrow-\infty$ in Eq. 32 and substituting the limit values from Eqs. 28b and 30:

$$\beta=\beta_{\text{in}}+\beta_{\text{out}} \quad (33)$$

where we defined:

$$\beta_{\text{in,out}}=\pm\frac{(-\Delta H)}{k_e^*}Gw_{\text{in,out}},\beta_{\text{in}}>\beta_{\text{out}}. \quad (34)$$

Equations 28b and 33 give a relation between w_{out} and T_m. Substituting C_{f0} from Eq. 32 into Eq. 24 gives:

$$\frac{d^2T_{f1}}{dv^2}=-a\left(\frac{dT_{f1}}{dv}-\beta_{\text{out}}\right)e^{T_{f1}/T_{f0}}, \quad (35)$$

where

$$a=\frac{\epsilon k_0\Pi e^{-E/RT_m}}{GE} \quad (36)$$

After integrating Eq. 35 between v and $-\infty$, we obtain:

$$\frac{dT_{f1}}{dv}-\beta+\beta_{\text{out}}\ln\left(\frac{\frac{dT_{f1}}{dv}-\beta_{\text{out}}}{\beta_{\text{in}}}\right)=-aT_{f0}e^{T_{f1}/T_{f0}} \quad (37)$$

Matching the first derivative of $0(1/\gamma)$ with the outer result, by taking the limit $v\rightarrow+\infty$, we get:

$$\beta+\beta_{\text{out}}\ln\left(\frac{\beta_{\text{in}}}{-\beta_{\text{out}}}\right)=\frac{\epsilon k_0\Pi T_m}{GE}e^{-E/RT_m}. \quad (38)$$

Since β, β_{out}, and β_{in} are known functions of the inlet conditions and T_m, the following relationships exists between the flow rate G and the maximum temperature, T_m:

$$G^2=\frac{\epsilon k_0\Pi T_m(k_e+bT_m^3)e^{-E/RT_m}}{E\left\{C_p(T_m-T_{\text{in}})+[w_{\text{in}}(-\Delta H)-C_p(T_m-T_{\text{in}})]\ln\left[1-\frac{C_p(T_m-T_{\text{in}})}{w_{\text{in}}(-\Delta H)}\right]\right\}}. \quad (39)$$

Discussion of adiabatic case

In Figure 2, G vs. T_m is shown both in the presence and absence of radiation. The other parameters have been taken as for CO oxidation and are listed in Table 1. As can be inferred from Figure 2, there exist a $G_{\min}$ and $G_{\max}$ and steady-state solutions only exist between these values. The radiation parameter b was chosen about ten times larger than realistic values to make its effect more apparent. Radiation tends to expand

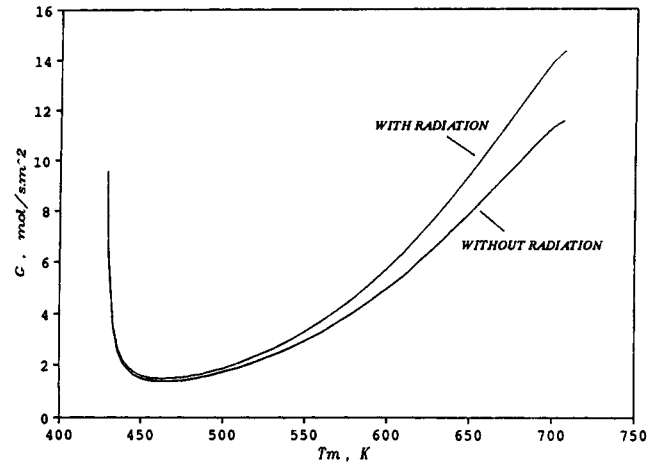

Figure 2. Maximum temperature vs. molar flow rate for adiabatic case.

the range of G and as is expected, the effect is more pronounced at higher temperatures. The critical values of G are associated with the blowoff and extinction flow rates. The blowoff condition occurs when w_{out} approaches zero. At that point, T_m reaches the theoretical adiabatic temperature T_{ad}, and the blowoff condition can be written as:

$$G_{\max}^2=\frac{\epsilon k_0(k_e+bT_{\text{ad}}^3)\Pi T_{\text{ad}}}{E(T_{\text{ad}}-T_{\text{in}})C_p}e^{-E/RT_{\text{ad}}}. \quad (40)$$

The accuracy of Eq. 40 was tested by integrating the governing Eqs. 1-5 numerically and checking for the maximum value of G for which a steady-state solution could be found. The numerical value was 15.5 mol/m^2·s, and Eq. 40 predicted a value of 14.3 mol/m^{2}s. This condition gives a good estimate of blowoff. Note that $w_{\text{out}}>0$ when $G<G_{\max}$. Also note that L_1 does not appear in any of the previous equations.

In Figure 3, the numerical solution is shown for the parameter values in Table 1. These are typical values for CO oxidation over CuO catalyst (Hlavacek and Vortruba, 1974). The temperature reaches a maximum at the outlet and has a value of 576.4 K, and the analysis predicts a value of 587.4 K, that is, an error of 7% in temperature rise. The numerical and analytical values for w_{out} are 0.014 and 0.013, respectively. In Figure 4, the numerical temperature profiles are shown with and without radiation. Radiation tends to decrease the maximum temperature, but it must be pointed out again that the parameter value of b was taken ten times larger than a realistic value and the effect of the radiation is not considered to be of major importance.

Some conclusions can be immediately drawn about G_m as computed by Eq. 40. The reaction rate constant and the thermal conductivity of the bed, including the radiation contribution, are proportional to G_m^2. Figure 5 shows that a higher adiabatic

Table 1. Parameter values

Item	Units	Case 1: CO Oxidation	Case 2: CH_4 Oxidation
b	$W/m \cdot K^4$	6.12×10^{-9}	—
C_p	$J/mol \cdot K$	30	66
d	m	0.023	0.04
ϵk_0	s^{-1}	4.48×10^9	9×10^7
E/R	K	11,524	15,000
G	$mol/s \cdot m^2$	5.0	2.6
h	$W/m^2 \cdot K$	—	20.0
k_e	$W/m \cdot K$	4.0	8.0
L_{total}	m	0.10	0.2
T_{in}	K	427	300
w_{in}	—	0.03	0.1
$-\Delta H$	J/mol	2.8×10^5	8.0×10^5
Π	atm	1.0	1.0

temperature rise broadens the range of molar flux for steady-state solutions, while a higher activation energy has the opposite effect.

Nonadiabatic system

When we consider nonadiabatic conditions, we unfortunately have to drop the contribution of radiation to keep the analysis tractable. But it followed from the discussion in the previous section that it plays a secondary role. The solution behind and ahead of the front has the general form:

$$T = T_{in} + A_{\pm} e^{M_1^{\pm} x} + B_{\pm} e^{M_2^{\pm} x} \tag{41}$$

where A_- and B_- are determined by the Danckwert's condition at the inlet and Eq. 23 at $x=0$. Likewise A_+ and B_+ are determined by Eq. 23 at $x=0$ and Eq. 8 at the outlet. $M_{1,2}^{\pm}$ are the solutions of the characteristic equation ahead and behind the front. When the molar flow rate does not change across the front (for example, methane and oxygen) the superscripts can be dropped. We further define two parameters:

$$\frac{dT}{dx_+} = \alpha = A_+ M_1^+ + B_+ M_2^+ \tag{42}$$

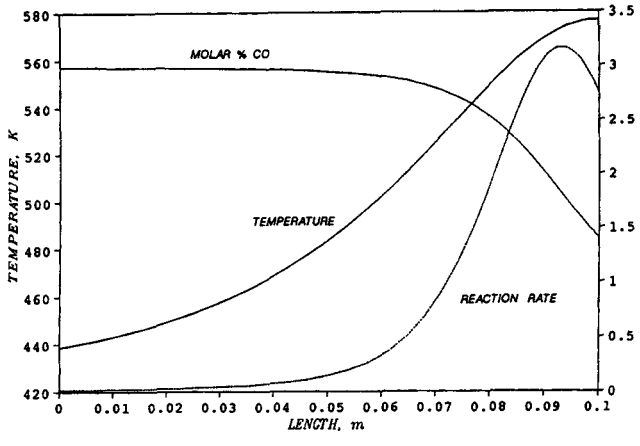

Figure 3. Numerical results for adiabatic CO oxidation.

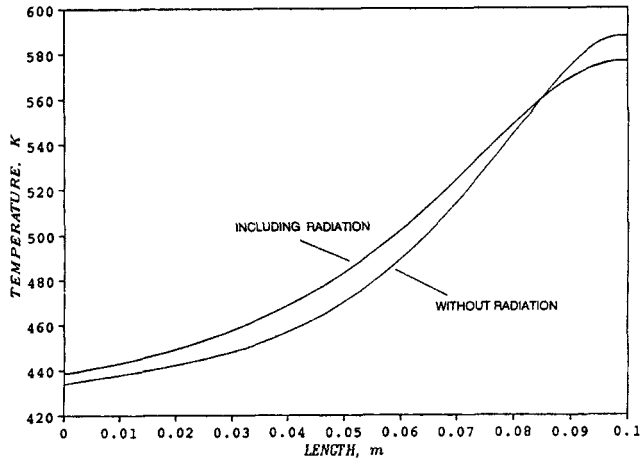

Figure 4. Effect of radiation on temperature for adiabatic CO oxidation.

$$\frac{dT}{dx_-} = \beta = A_- M_1^- + B_- M_2^- . \tag{43}$$

The analysis of the flame zone follows in the same way as for the adiabatic case. The only difference is the boundary conditions, when $v \to +\infty$:

$$T_{f1} \to -\infty, \quad \frac{dT_{f1}}{dv} = \alpha \tag{44}$$

and β_{out} is redefined as:

$$\beta_{out} = \alpha - \frac{G(-\Delta H) w_{out}}{k_e} . \tag{45}$$

The temperature drops at both sides of the reaction zone which implies a local maximum. Then, at $v=0$ we have:

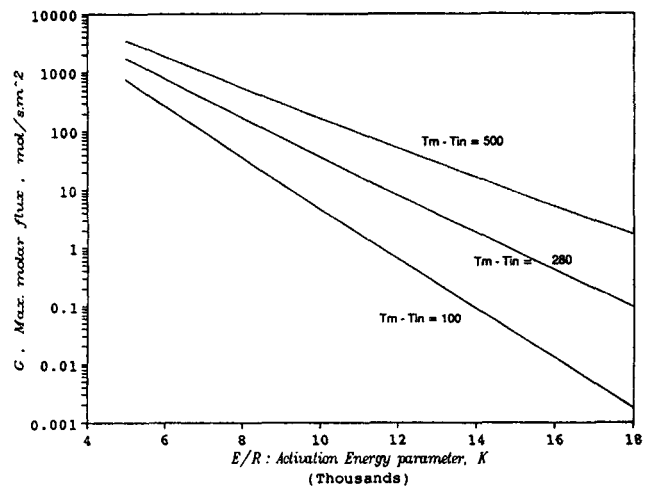

Figure 5. Effect of activation energy and temperature rise on maximum flow rate.

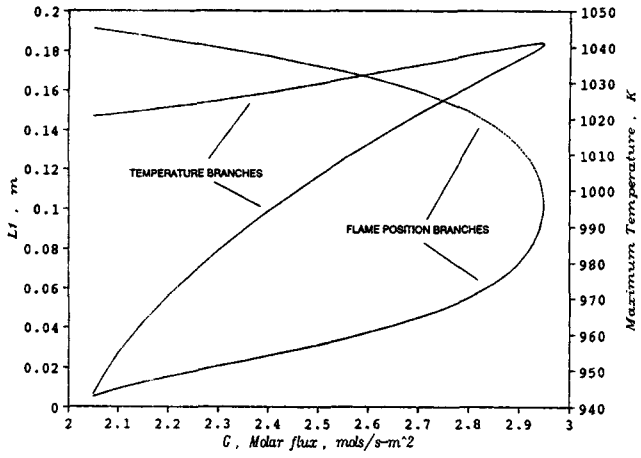

Figure 6. Flame position and maximum temperature vs. flow rate: nonadiabatic case.

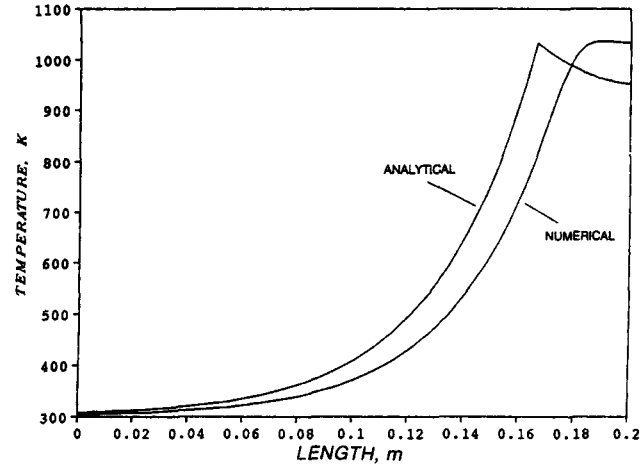

Figure 8. Analytical and numerical temperature profiles: reaction front near outlet.

$$T_{f1}=0,\ \frac{dT_{f1}}{dv}=0 \tag{46}$$

But Eq. 37 still holds, and we can substitute the values for T_{f1} and dT_{f1}/dv at $v=0$ and at $v\to+\infty$ to get:

$$\beta+(\beta_{in}-\beta)\ln\left(1-\frac{\beta}{\beta_{in}}\right)=\frac{\epsilon k_0\Pi T_m}{GE}\,e^{-E/RT_m} \tag{47}$$

$$\beta-\alpha=(\beta_{in}-\beta)\ln\left(\frac{w_{in}}{w_{out}}\right). \tag{48}$$

Discussion of Nonadiabatic case

Equations 33, 42, 43, 47, and 48 have to be solved simultaneously for the unknowns, α, β, T_m, w_{out}, and L_1. Note that both α and β as defined by Eqs. 42 and 43 are functions of L_1. Blowoff occurs when the system of equations does not have a realistic solution for L_1, and the critical value of G_m is reached.

The noncatalytic oxidation of CH_4 as reported by Sathe et al. (1990) has been chosen as an example, as shown in Table 1. Figure 6 is a bifurcation diagram that shows the analytical results for the two possible positions of the steady state as a function of the molar flow rate. This figure was constructed by solving simultaneously Eqs. 33, 42, 43, 47, and 48 using the data of Table 1. for $G<2.05$ and $G>2.95$, no solution exists. For G within this rather narrow interval, two flame positions can exist, one warmer and closer to the outlet and the other colder and closer to the inlet. Both branches meet at $G_m=2.95$ and $T=997$ K. This critical point is a turning point. Also shown is the maximum temperature at each flame position. Note that the maximum temperature is higher when the flame is located near the outlet and cooler when it is closer to the inlet.

These observations are confirmed by the numerical results, as shown in Figures 7 and 8 for a value of $G=2.6$ mol/s m^{2}s. Figure 7 shows the numerical and analytical temperature profiles for the flame located closer to the inlet, and Figure 8 shows the case when the flame is located closer to the outlet. Both the numerical and analytical results indicate that the maximum temperature is lower when the flame is located closer to the inlet. The maximum temperature, conversion and L_1 tend to be overestimated. For example, for the solution closer to the inlet we found numerically $T_m=990$ K, $L_1=0.019$ m, and $w_{out}=0.0043$. The corresponding analytical values are $T_m=1{,}013$ K, $L_1=0.037$ m, and $w_{out}=0.0019$.

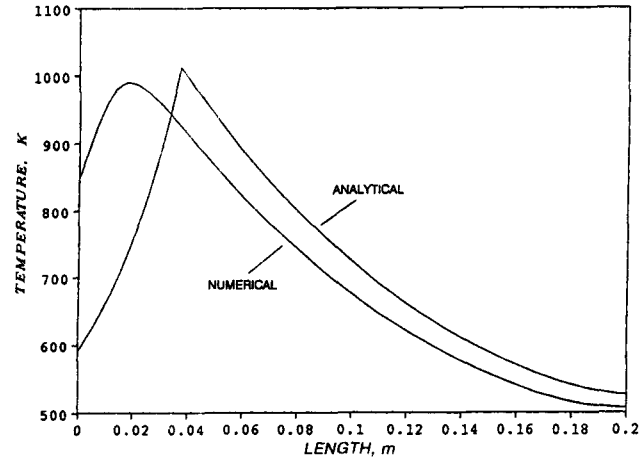

Figure 7. Analytical and numerical temperature profiles: reaction front near inlet.

Conclusions

The steady-state solution for a reaction with sharp profile in a porous medium was determined for two situations: an adiabatic system including radiation effects and the nonadiabatic case without radiation.

In the adiabatic case, the reaction front is located right at the outlet. The radiation tends to lower both the maximum temperature and the conversion. The maximum molar flux before blowout occurs is enhanced by higher reaction rate constants, larger radiation effects, and a larger temperature rise (higher enthalpy of reaction, higher inlet reactant concentration, and so on) but it is decreased significantly by higher activation energies. The analytical model predicted the max-

imum temperature, conversion and maximum molar flux within 10% of the numerical results.

For the nonadiabatic system, the analytical model predicted two steady-state solutions and it was confirmed by the numerical results. But the quantitative agreement between the analytical and numerical solutions decreased, probably due to an increase in the reaction zone thickness.

Notation

a = constant, Eq. 36
A = constant, Eq. 41
b = $4\phi\sigma_B d_p$
B = constant, Eq. 41
c = $\rho UCp\epsilon$
C = concentration of reactant
C_p = specific heat
d = tube diameter
d_p = particle size in bed
E = activation energy
G = molar flux
h = heat-transfer coefficient
$(-\Delta H)$ = heat of reaction
k_e, k_e^* = thermal conductivity
k_0 = frequency factor
L_{tot} = length of reactor
$M_{1,2}$ = roots of characteristic equation
R = universal gas constant
T = temperature
U = velocity
v = expanded axial distance
w = reactant molar fraction
x = axial distance

Greek letters

α = defined by Eq. 42
β = defined by Eqs. 16 and 43
γ = E/RT_m
ϵ = porosity
Π = absolute inlet pressure
ρ = molar density
σ_B = Stefan-Boltzmann constant
ϕ = radiation transfer factor

Subscripts

ad = adiabatic
+ = downstream of flame
− = upstream of flame
f = inner expansion
g = gas
in = inlet
m = maximum value
out = outlet

Literature Cited

Gatica, J. E., J. Puszynski, and V. Hlavacek, "Reaction Front Propagation in Nonadiabatic Exothermic Reaction Flow Systems," *AIChE J.*, **33**(5), 819 (1987).

Golombok, M., H. Jariwala, and L. C. Shirvill, "Gas-Solid Heat Exchange in a Fibrous Metallic Material Measured by a Heat Regenerator Technique," *Int. J. Heat Mass Transfer*, **33**(2), 243 (1990).

Hlavacek, V., "Aspects in Design of Packed Catalytic Reactors," *Ind. Eng. Chem. Fund.*, **62**(7), 8 (1970).

Hlavacek, V., and J. Votruba, "Experimental Study of Multiple Steady States in Adiabatic Catalytic Systems," *Adv. in Chemistry Ser.*, **133**(5), 545 (1974).

Matkowsky, B. J., and G. I. Sivashinsky, "Acceleration Effects on the Stability of Flame Propagation," *SIAM J. Appl. Math.*, **37**(3) 669 (1979).

Marquardt, W., "Wave Propagation Phenomena in Chemical Engineering Processes," *Chem. Ing. Tech.*, **61**(5), 362 (1989).

Norbury, J., and A. M. Stuart, "A Model for Porous-Medium Combustion," *Quart. J. Mech. Appl. Math.*, **42**, 159 (1989).

Sathe, S. B., R. E., and T. W. Tong, "A Numerical Analysis of Heat Transfer and Combustion in Porous Radiant Burners," *Int. J. Heat Mass Transfer*, **33**(6), 1331 (1990).

Sparrow, E. M., and R. D. Cess, *Radiation Heat Transfer*, Brooks/Cole Publishing, Beltmont, CA (1970).

Thiart, J. J., H. J. Viljoen, K. Kriel, J. E. Gatica, and V. Hlavacek, "Development of Thermal Stresses in Reacting Media I: Failure of Catalyst Particle," *Chem. Eng. Sci.*, **46**(1), 351 (1991).

Thiart, J. J., S. M. Bradshaw, H. J. Viljoen, and V. Hlavacek, "Thermo-Chemical Stress Development in Ceramic Catalyst Supports: II," *Chem. Eng. Sci.*, in press (1993).

Viskanta, R., and M. P. Menguc, "Radiative Transfer in Dispersed Media," *Appl. Mech. Rev.*, **42**(9), 241 (1989).

Vortmeyer, D., "Radiation in Packed Solids," *Ger. Chem. Eng.*, **3**(2), 124 (1980).

Manuscript received Aug. 26, 1992, and revision received Mar. 5, 1993.